

The long non-coding RNA ANRIL promotes proliferation and cell cycle progression and inhibits apoptosis and senescence in epithelial ovarian cancer

Jun-jun Qiu^{1,2,3}, Yan Wang^{4,5}, Ying-lei Liu⁶, Ying Zhang^{1,2,3}, Jing-xin Ding^{1,2,3}, Ke-qin Hua^{1,2,3}

¹Department of Gynecology, Obstetrics and Gynecology Hospital, Fudan University, Shanghai, China

²Department of Obstetrics and Gynecology of Shanghai Medical College, Fudan University, Shanghai, China

³Shanghai Key Laboratory of Female Reproductive Endocrine-Related Diseases, Fudan University, Shanghai, China

⁴Cancer Institute, Shanghai Medical College, Fudan University, Shanghai, China

⁵Department of Oncology, Shanghai Medical College, Fudan University, Shanghai, China

⁶Department of Gynecology, The Second Affiliated Hospital of Nantong University, Nantong, China

Correspondence to: Ke-qin Hua, **email:** huakeqin@126.com

Keywords: ANRIL, proliferation, cell cycle, apoptosis, senescence

Received: September 03, 2015

Accepted: February 16, 2016

Published: April 15, 2016

ABSTRACT

Antisense non-coding RNA in the INK4 locus (ANRIL) has been implicated in a variety of cancers. In the present study, we evaluated ANRIL expression in epithelial ovarian cancer (EOC) and defined its clinical implications and biological functions. ANRIL was overexpressed in EOC tissues relative to normal controls. Overexpression correlated with advanced International Federation of Gynecologists and Obstetricians stage and high histological grade. Multivariate analysis indicated that ANRIL is an independent prognostic factor for overall survival in EOC. Gain- and loss-of-function experiments demonstrated that ANRIL promotes EOC cell proliferation both *in vitro* and *in vivo*. The proliferative effect was linked to the promotion of cell cycle progression and inhibition of apoptosis and senescence. Down-regulation of P15^{INK4B} and up-regulation of Bcl-2 by ANRIL may partially explain ANRIL-induced EOC cell proliferation. This study is the first to establish that ANRIL promotes EOC progression and is a potential prognostic biomarker.

INTRODUCTION

Epithelial ovarian cancer (EOC) is one of the most aggressive malignancies [1–3]. The prognosis of EOC is very poor, primarily because it is typically diagnosed at an advanced stage and because of the lack of efficacious therapies [3]. Despite extensive clinical and basic research, the overall survival (OS) rate has not improved [4, 5]. A better understanding of the molecular mechanisms involved in EOC progression may facilitate the identification of novel markers and effective therapeutic strategies that can prolong survival and improve patient outcomes.

Mounting evidence indicates that the molecular mechanisms of carcinogenesis and cancer progression involve not only to protein-coding genes, but also non-coding RNAs. Long non-coding RNAs (lncRNAs, > 200 nucleotides) were initially thought to be the “dark

matter” of the genome but have recently emerged as critical components of the cancer transcriptome [6, 7]. Many lncRNAs control carcinogenesis and cancer progression, and potentially represent a new avenue for cancer research [8–17]. Elucidation of the roles of these lncRNAs will provide insight into the molecular biology underlying cancer initiation and progression.

Recently, antisense non-coding RNA in the INK4 locus (ANRIL) has garnered substantial attention. ANRIL is transcribed as a 3.8-kb lncRNA in the antisense orientation of the INK4b/ARF/INK4a gene cluster [18]. ANRIL was initially identified in a genetic analysis of familial melanoma patients with neural tumors [19]. It was subsequently determined to be independently associated on a genome-wide level with several other forms of cancer including breast cancer [20], pancreatic carcinoma [21], nasopharyngeal carcinoma [22], basal cell carcinoma [23],

glioma [24], leukemia [25], prostate cancer [26], esophageal squamous cell carcinoma [27] and gastric cancer [28]. We recently linked ANRIL to metastasis in serous ovarian cancer (SOC), a histotype of EOC [29]. However, the role of ANRIL in EOC has not been determined and an association between ANRIL and other aspects of EOC progression in addition to metastasis has not been demonstrated.

In the present study, we investigated the expression pattern, clinical significance, and biological functions of ANRIL in EOC including proliferation, cell cycle progression, apoptosis, and senescence. We demonstrated that ANRIL levels were elevated in EOC tissues compared with normal controls and that ANRIL serves as an independent predictor of overall survival (OS) in EOC patients. We also determined that ANRIL promotes EOC cell proliferation both *in vitro* and *in vivo*. This effect on proliferation was associated with the promotion of cell cycle progression and inhibition of both apoptosis and senescence. Down-regulation of P15^{INK4B} and up-regulation of Bcl-2 by ANRIL may partially explain ANRIL-induced EOC cell proliferation. Our study is the first to establish that ANRIL contributes to EOC progression and that ANRIL has the potential to be a novel biomarker for predicting poor survival in EOC patients.

RESULTS

Overexpression of ANRIL is correlated with FIGO stage, histological grade, and poor prognosis in EOC

We showed that ANRIL expression was significantly elevated in 102 EOC tissues compared with 30 noncancerous tissues using qRT-PCR ($P < 0.01$; Figure 1A). The median relative ANRIL expression value was used as a cut-off [14] to divide the 102 EOC patients into a high-ANRIL group ($n = 51$; an ANRIL level \geq the median value) and a low-ANRIL group ($n = 51$; an ANRIL level $<$ the median value). An examination of the correlation between ANRIL expression and clinicopathological features revealed that increased ANRIL expression was correlated with advanced FIGO stage and high histological grade, but not with age, histological type, residual tumor diameter, CA-125 level, or ascites (Table 1). These results suggested that ANRIL overexpression was associated with a more malignant ovarian cancer phenotype.

To evaluate survival, univariate log-rank tests and multivariate Cox regression analyses were performed. As shown in Figure 1B and Table 2, OS was significantly shorter for patients with high ANRIL expression compared to those with low expression ($P < 0.01$). Additionally, the multivariate analyses revealed that ANRIL expression, FIGO stage, and histological grade were independent predictors of OS ($P < 0.01$, Table 2). Based on these data, we concluded that ANRIL could serve as a

predictive biomarker for EOC outcome and that ANRIL overexpression may contribute to EOC progression.

ANRIL knockdown inhibits EOC cell proliferation *in vitro*

Based on the association of ANRIL with a more malignant cancer phenotype in EOC, we hypothesized that ANRIL was involved in EOC cell proliferation. We therefore examined ANRIL levels in six EOC cell lines. Of these cell lines, the A2780 and OVCA433 cells exhibited the highest ANRIL expression (Figure 2A) and were selected for further loss-of-function experiments. Because both siRNAs efficiently silenced ANRIL expression in these cell lines (Figure 2B), we designed lentiviral vectors to establish stable ANRIL knockdown cell lines (A2780-KD1, A2780-KD2, OVCA433-KD1, and OVCA433-KD2 cells) and the corresponding controls (A2780-NC and OVCA433-NC cells).

To assess the effects of ANRIL on EOC cell proliferation *in vitro*, we performed MTT and colony formation assays. MTT assays demonstrated that A2780-KD and OVCA433-KD cells proliferated more slowly than A2780-NC and OVCA433-NC cells (Figure 2C). In addition, there were fewer A2780-KD and OVCA433-KD colonies compared to A2780-NC and OVCA433-NC colonies (Figure 2D). These results suggested that ANRIL knockdown inhibited EOC cell proliferation *in vitro*.

ANRIL knockdown inhibits cell cycle progression and promotes apoptosis and senescence

To explore the cause of the growth inhibition following ANRIL-knockdown, we evaluated the effect of ANRIL on cell cycle progression. Flow cytometry results indicated that the proportion of cells in S phase decreased in both A2780-KD and OVCA433-KD cells compared with the corresponding controls (Figure 3A), suggesting that ANRIL knockdown blocked cell cycle progression.

Given that a decrease in cell death (including cell death due to apoptosis) is one of the primary mechanisms underlying tumor growth, we evaluated the effect of ANRIL on apoptosis. ANRIL knockdown increased the total number of apoptotic cells in both the A2780-KD and OVCA433-KD cell lines compared to the corresponding controls (Figure 3B), indicating that ANRIL knockdown could promote apoptosis. We also investigated the effect of ANRIL on cell senescence since inducing senescence is an important strategy for arresting proliferation of oncogenic cells. The proportion of cells that were positive for β -galactosidase activity, an indicator of cell senescence, was increased in the A2780-KD and OVCA433-KD cell lines compared to the corresponding controls (Figure 3C), suggesting that ANRIL silencing

may promote senescence. These results demonstrated that the inhibitory effect on proliferation induced by ANRIL silencing was partially due to the inhibition of cell cycle progression and the promotion of apoptosis and senescence.

Overexpression of ANRIL enhances EOC cell proliferation and cell cycle progression and inhibits apoptosis and senescence

We next performed gain-of-function experiments to further elucidate the effects of ANRIL on proliferation, cell cycle progression, apoptosis, and senescence. We established stable OVCA429-OE cells because this cell line exhibited the lowest ANRIL expression of the cell lines examined (Figure 2A). The efficiency of ANRIL overexpression was confirmed using qRT-PCR (Figure 4A). MTT and colony formation assays showed that overexpression of ANRIL increased OVCA429 cell proliferation (Figure 4B, 4C). Flow cytometry analysis revealed that overexpression of ANRIL promoted cell cycle progression by enhancing the proportion of OVCA429 cells in S phase (Figure 4D). Apoptosis assays showed that overexpression of ANRIL decreased the total number of apoptotic OVCA429 cells (Figure 4E). Senescence assays demonstrated that population of cells positive for β -galactosidase activity decreased in OVCA429-OE cells (Figure 4F). These results indicated that overexpression of ANRIL enhanced EOC cell proliferation partially through the promotion of cell cycle progression and the inhibition of apoptosis and senescence.

P15 and Bcl-2 are key genes downstream of ANRIL that promote EOC cell proliferation

ANRIL inhibits neighboring tumor suppressors (P14^{ARF}, P15^{INK4B}, and P16^{INK4A}), which can impair cell cycle progression and influence key physiological

processes including senescence and apoptosis [18, 30]. Thus, we examined whether ANRIL altered the expression of P14^{ARF}, P15^{INK4B}, and P16^{INK4A} in EOC cells. Western blotting demonstrated that ANRIL knockdown in A2780 and OVCA433 cells increased P15^{INK4B} but not P16^{INK4A} or P14^{ARF} protein levels (Figure 5A). We also examined the expression of Bcl-2 and survivin, since both are central regulators of apoptosis and contribute to tumor progression [31, 32]. Western blotting demonstrated that ANRIL silencing in A2780 and OVCA433 cells decreased the level of Bcl-2 but not survivin (Figure 5A). We then analyzed the expression of P15^{INK4B} and Bcl-2 in OVCA429-OE cells by western blotting. ANRIL overexpression decreased P15^{INK4B} but increased Bcl-2 protein levels (Figure 5B). Consistent with these results, increased P15^{INK4B} and decreased Bcl-2 mRNA levels were detected in A2780-KD and OVCA433-KD cells, while decreased P15^{INK4B} and increased Bcl-2 mRNA levels were detected in OVCA429-OE cells (Figure 5C). These results suggested that ANRIL promoted EOC cell proliferation in part by decreasing P15^{INK4B} and increasing Bcl-2 levels.

Interestingly, we found that ANRIL knockdown in A2780 and OVCA433 cells increased the levels of apoptosis markers such as caspase-9 and caspase-3, but not caspase-7. In contrast, ANRIL overexpression decreased the levels of caspase-9 and caspase-3 but not caspase-7 (Supplementary Figure S1). These results are consistent with previous studies, which reported that ANRIL inhibits caspase-9 and caspase-3 expression in bladder cancer [33].

ANRIL contributes to EOC tumor growth *in vivo*

We further examined the effects of ANRIL on EOC cell proliferation *in vivo*. A2780-KD1, A2780-KD2, and A2780-NC cells were injected into nude mice and tumor

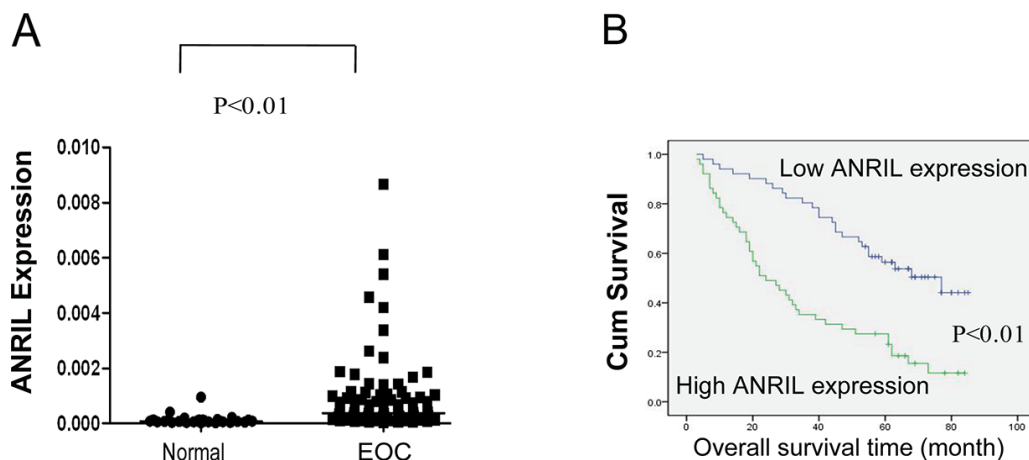


Figure 1: Relative ANRIL expression levels and their association with poor prognosis in EOC. (A) Relative ANRIL expression levels in EOC and normal ovarian tissues. (B) Kaplan-Meier analysis of OS was performed based on ANRIL expression levels.

Table 1: Association of ANRIL expression with clinicopathological variables in EOC patients

Variables	Low ANRIL expression (n = 51)	High ANRIL expression (n = 51)	P
	n (%)	n (%)	
Age (years)			
< 50	18 (43.9)	23 (56.1)	0.313
≥ 50	33 (54.1)	28 (45.9)	
Histological subtype			
Serous	31 (45.6)	37 (54.4)	0.208
Other	20 (58.8)	14 (41.2)	
FIGO stage			
I–II	25 (75.8)	8 (24.2)	< 0.001
III–IV	26 (37.7)	43 (62.3)	
Histological grade			
G1-G2	25 (67.6)	12 (32.4)	0.007
G3	26 (40.0)	39 (60.0)	
Residual tumor diameter (cm)			
< 1	24 (47.2)	18 (52.8)	0.385
≥ 1	27 (56.7)	33 (43.3)	
CA125 level (U/ml)			
< 600	38 (57.1)	24 (42.9)	0.227
≥ 600	13 (45.0)	27 (55.0)	
Ascites			
< 100	24 (58.5)	17 (41.5)	0.157
≥ 100	27 (44.3)	34 (55.7)	

growth was analyzed. The tumors formed by A2780-KD1 and A2780-KD2 cells were smaller in both size and weight compared to A2780-NC tumors (Figure 6A, 6B and 6C). Immunohistochemical staining revealed that tumor nodules originating from A2780-KD1 and A2780-KD2 cells had decreased ki67, increased P15^{INK4B}, and decreased Bcl-2 expression compared to nodules originating from A2780-NC cells (Figure 6D). These results were consistent with the *in vitro* studies and confirmed that ANRIL contributed to EOC tumor growth *in vivo* in part through down-regulation of P15^{INK4B} and up-regulation of Bcl-2.

DISCUSSION

The involvement of lncRNAs in tumor processes such as proliferation, apoptosis, and metastasis reinforces the roles of these transcripts in cancer progression and suggests that they may be prognostic biomarkers. Indeed,

HOTAIR was identified as a prognostic marker of metastasis in diverse human cancers [34–38]. MALAT-1 promotes metastasis and serves as a prognostic indicator in lung cancer [10]. GAS5 inhibits proliferation and serves as a prognostic indicator in hepatocellular and colorectal cancer [39, 40]. Here, we have reported the first evidence indicating that ANRIL is overexpressed in EOC tissues. ANRIL overexpression was correlated with advanced FIGO stage and high histological grade. Moreover, univariate and multivariate survival analyses demonstrated that ANRIL could serve as an independent prognostic indicator. These clinical findings highlight the potential value of ANRIL as a novel prognostic marker for EOC and suggest that ANRIL contributes to EOC progression.

ANRIL has been implicated in many human solid carcinomas [19–25, 27, 28]. Although our previous study linked ANRIL to metastasis in SOC, it was not clear whether ANRIL contributed to EOC and whether it was

Table 2: Univariate and multivariate analysis of overall survival in 102 EOC patients

Variables	Univariate analysis		Multivariate analysis					
	Overall survival (months)	P	Overall survival					
	Mean ± SE		β	SE	Wald	P	Exp (β)	95% CI
Age (years)								
< 50	45.60 ± 4.37	0.634	—	—	—	—	—	—
≥ 50	49.01 ± 3.81		—	—	—	—	—	—
Histological subtype								
Serous	48.56 ± 3.45	0.839	—	—	—	—	—	—
Other	47.36 ± 5.51		—	—	—	—	—	—
CA125 level (U/ml)								
< 600	53.86 ± 4.44	0.131	—	—	—	—	—	—
≥ 600	43.97 ± 3.81		—	—	—	—	—	—
Ascites								
< 100	55.23 ± 4.49	0.075	—	—	—	—	—	—
≥ 100	43.28 ± 3.75		—	—	—	—	—	—
FIGO stage								
I–II	77.51 ± 2.48	< 0.001	—	—	—	—	—	—
III–IV	33.68 ± 2.84		1.958	0.461	18.084	< 0.001	7.089	2.874–17.482
Histological grade								
G1–G2	66.45 ± 4.34	< 0.001	—	—	—	—	—	—
G3	37.43 ± 3.19		0.865	0.319	7.348	0.007	2.375	1.271–4.439
Residual tumor diameter (cm)								
< 1	52.39 ± 3.60	0.01	—	—	—	—	—	—
≥ 1	38.44 ± 4.65		0.478	0.270	3.129	0.077	1.613	0.950–2.738
ANRIL expression								
Low	61.71 ± 3.68	<	—	—	—	—	—	—
High	34.62 ± 3.73	0.001	0.656	0.278	5.574	0.018	1.928	1.118–3.324

β: Regression coefficient; SE: Standard error; CI: confidence interval.

associated with other aspects of EOC progression in addition to metastasis. In the present study, we showed that ANRIL depletion in A2780 and OVCA433 cells inhibited proliferation, delayed cell cycle progression, and promoted apoptosis and senescence. In contrast, overexpression of ANRIL in OVCA429 cells enhanced proliferation, promoted cell cycle progression, and inhibited apoptosis and senescence. Additionally, *in vivo* experiments confirmed that ANRIL knockdown inhibited tumor growth in nude mice. These data suggest that

ANRIL is an important factor in promoting EOC growth and that ANRIL likely promotes cell cycle progression and inhibits apoptosis and senescence to drive tumor growth.

The downstream molecular events by which ANRIL promotes EOC cell proliferation are not yet clear. ANRIL inhibits P14^{ARF} (a regulator of the p53 pathway), P15^{INK4B}, and P16^{INK4A} (two cyclin-dependent kinase inhibitors), which are neighboring tumor suppressors [18]. P15^{INK4B} has a well-described role in proliferation, cell cycle progression, and replicative senescence

[18, 30]. Consistent with these previous findings, our data demonstrated that ANRIL decreased P15^{INK4B} protein and mRNA levels, suggesting that ANRIL may promote EOC cell cycle progression, inhibit senescence, and enhance proliferation partially through decreasing P15^{INK4B} levels. Given the evidence suggesting that ANRIL can also act on specific genes independently of P14^{ARF}/P15^{INK4B}/

P16^{INK4A} [41, 42], we investigated whether ANRIL altered the expression of Bcl-2 and survivin, two central regulators of proliferation and apoptosis. As expected, ANRIL silencing decreased Bcl-2 protein and mRNA levels while overexpression of ANRIL increased Bcl-2 protein and mRNA levels. These results are consistent with previous data indicating that ANRIL knockdown

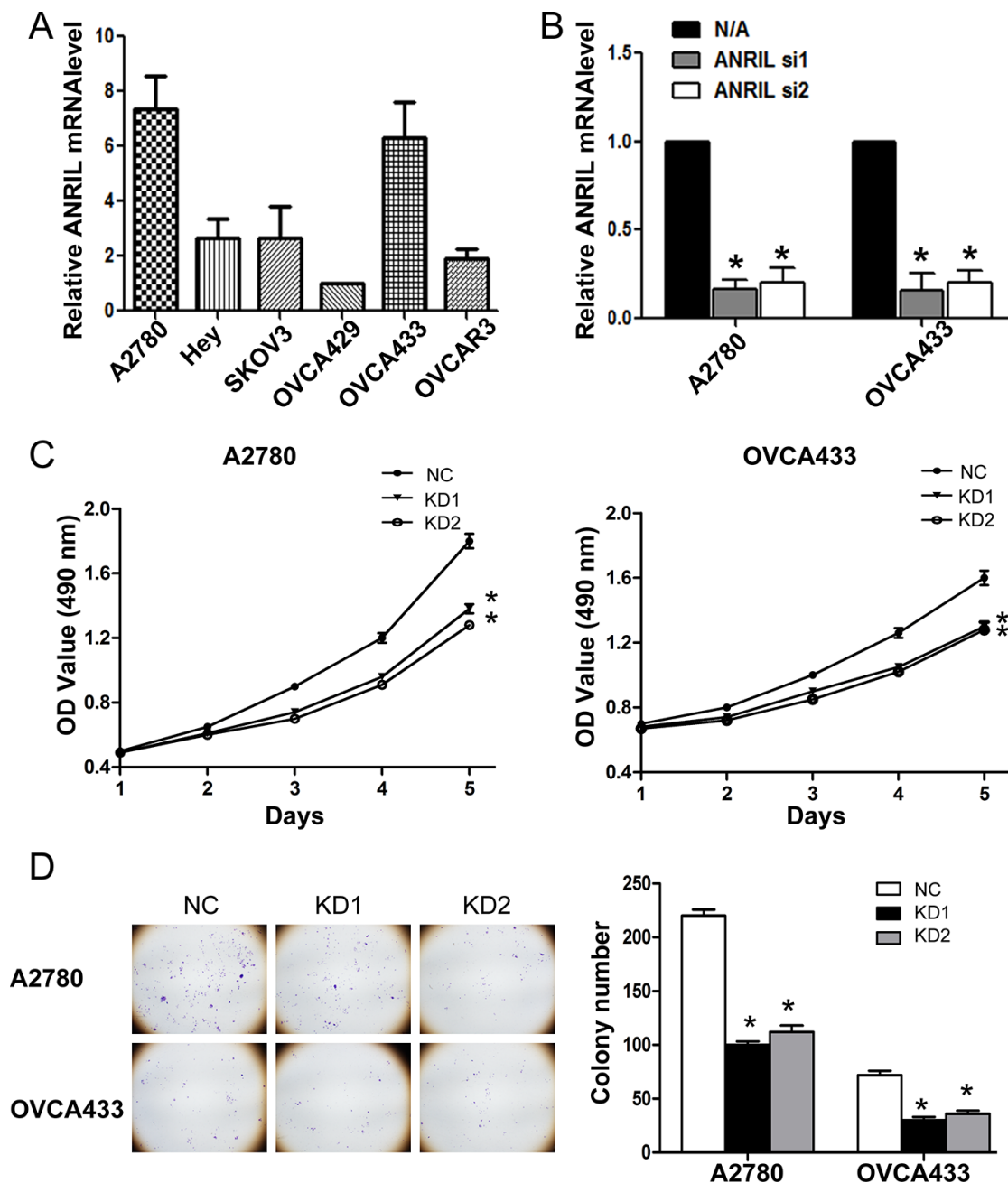


Figure 2: ANRIL knockdown inhibits the proliferation of A2780 and OVCA433 cells. (A) Relative ANRIL expression levels in EOC cell lines (A2780, Hey, SKOV3, OVCA429, OVCA433, and OVCAR3). (B) Relative ANRIL expression levels in A2780 and OVCA433 cells transfected with si-NC or ANRIL siRNAs. * $P < 0.05$. (C) MTT assays were performed to evaluate the proliferation of A2780-KD and OVCA433-KD cells compared to controls. The data represent the mean \pm standard deviation (SD) of three independent experiments. Bars denote the SD. * $P < 0.05$. (D) Representative colony formation assay results for A2780-KD and OVCA433-KD cells and corresponding controls. * $P < 0.05$.

repressed proliferation and promoted apoptosis in bladder cancer by reducing Bcl-2 levels [33]. *In vivo* experiments confirmed that ANRIL promoted EOC tumor growth in part by decreasing P15^{INK4B} and increasing Bcl-2 levels. Insight into the mechanisms by which ANRIL alters P15^{INK4B} and Bcl-2 expression was provided by a previous

study that showed that ANRIL depletion could disrupt SUZ12, a component of the polycomb repressive complex 2 (PRC2), by binding to the P15^{INK4B} locus and increasing P15^{INK4B} expression [43]. Additionally, a recent study reported that P15^{INK4B} down-regulated Bcl-2 expression in chronic myeloid leukemia cells [44]. Collectively, our

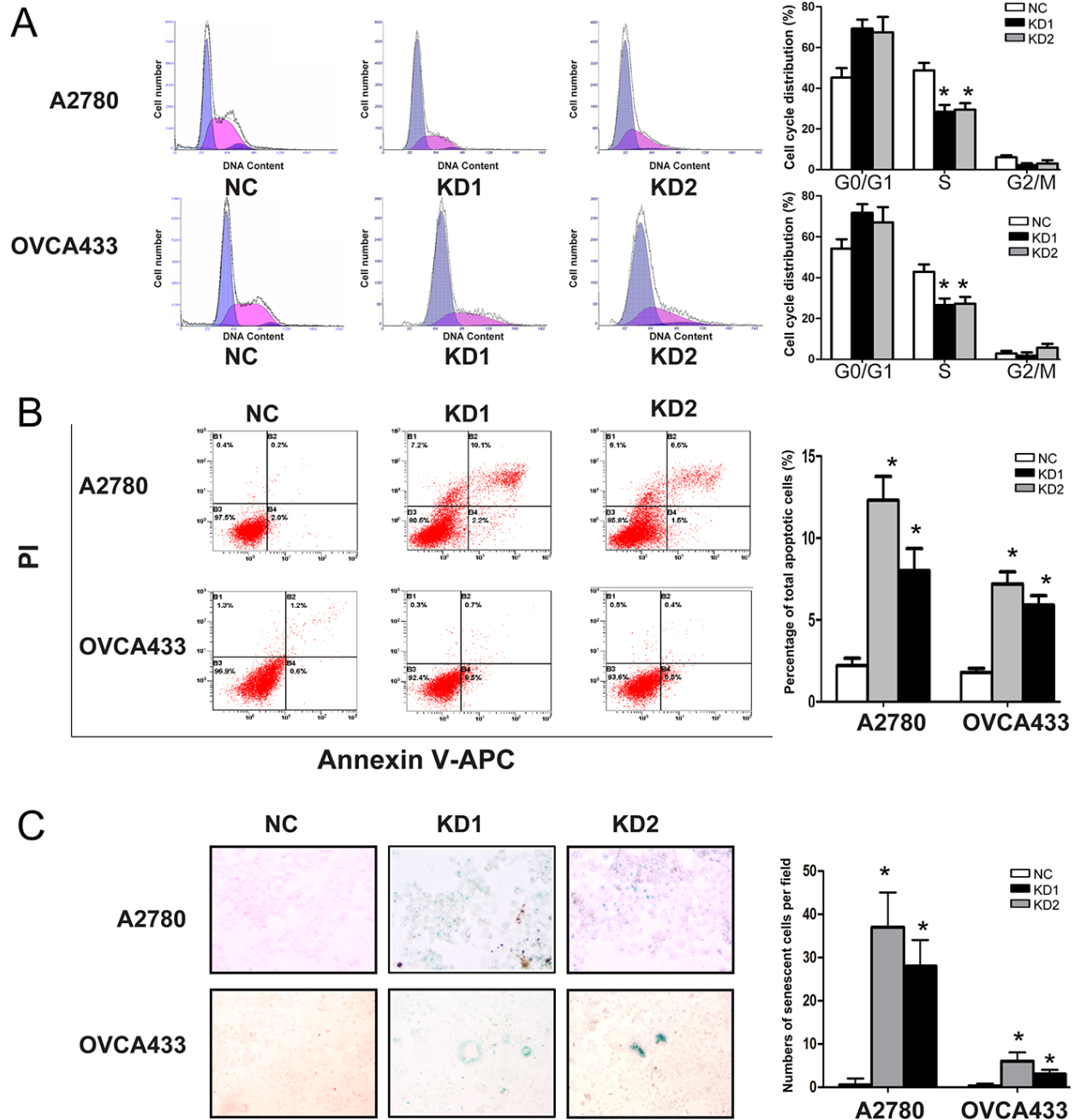


Figure 3: ANRIL knockdown inhibits cell cycle progression and promotes apoptosis and senescence in A2780 and OVCA433 cells. (A) Cell cycle analysis was performed using flow cytometry. The bar graph on the right presents the percentage of cells in the G0-G1, S, or G2-M phases of the cell cycle. Representative histograms are presented on the left. The results shown are representative of three independent experiments. * $P < 0.05$. (B) Apoptosis was assessed using flow cytometry. The bar graph on the right presents the percentage of apoptotic cells. Representative quadrant figures are presented on the left. The results shown are representative of three independent experiments. * $P < 0.05$. (C) Cells were stained with the senescence marker β -galactosidase. The blue staining around the nucleus in A2780-KD and OVCA433-KD cells indicates cellular senescence. * $P < 0.05$.

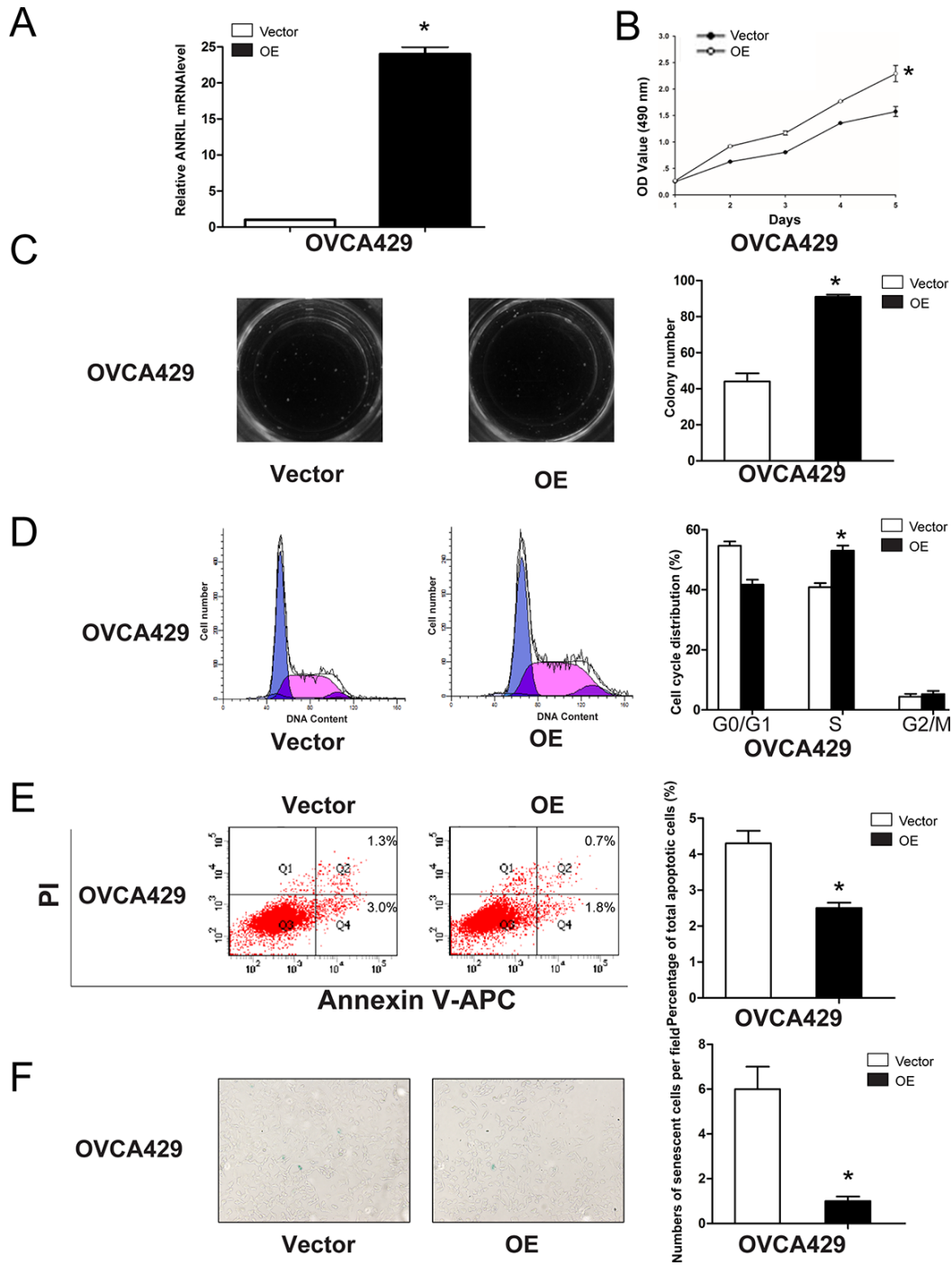


Figure 4: Overexpression of ANRIL promotes EOC cell proliferation and cell cycle progression, and inhibits apoptosis and senescence in OVCA429 cells. (A) Relative ANRIL expression levels in OVCA429-OE cells and control cells. $*P < 0.05$. (B) MTT assays were performed to evaluate the proliferation of OVCA429-OE and OVCA429-Vector cells. $*P < 0.05$. (C) Representative colony formation assay results for OVCA429-OE and OVCA429-Vector cells. $*P < 0.05$. (D) Cell cycle analysis was performed using flow cytometry in OVCA429-OE and OVCA429-Vector cells. The bar graph on the right presents the percentage of cells in the G0–G1, S, or G2-M phases of the cell cycle. $*P < 0.05$. (E) Apoptosis was assessed using flow cytometry. The bar graph on the right presents the percentage of apoptotic cells. $*P < 0.05$. (F) OVCA429-OE and OVCA429-Vector cells were stained with β -galactosidase. The blue staining around the nucleus indicates cellular senescence. $*P < 0.05$.

data and the previous findings suggest that P15^{INK4B} and Bcl-2 are key genes downstream of ANRIL that promote EOC cell proliferation. A limitation of the present study was that we did not investigate the exact mechanism involving “ANRIL-P15^{INK4B}-Bcl-2”. Thus, further studies are required to elucidate the underlying molecular mechanisms.

In summary, our clinical data demonstrated that ANRIL was overexpressed in EOC, which was correlated with FIGO stage, and could serve as an independent predictor for OS. Moreover, gain- and

loss-of-function studies demonstrated that ANRIL promoted EOC cell proliferation both *in vitro* and *in vivo*, and that the proliferative effect was linked to the promotion of cell cycle progression and inhibition of apoptosis and senescence. Finally, we demonstrated that ANRIL decreased P15^{INK4B} and increased Bcl-2 expression, which may partially account for ANRIL-induced EOC cell proliferation. Our study is the first to establish that ANRIL promotes EOC progression and that it may be a biomarker that can be used to predict poor survival.

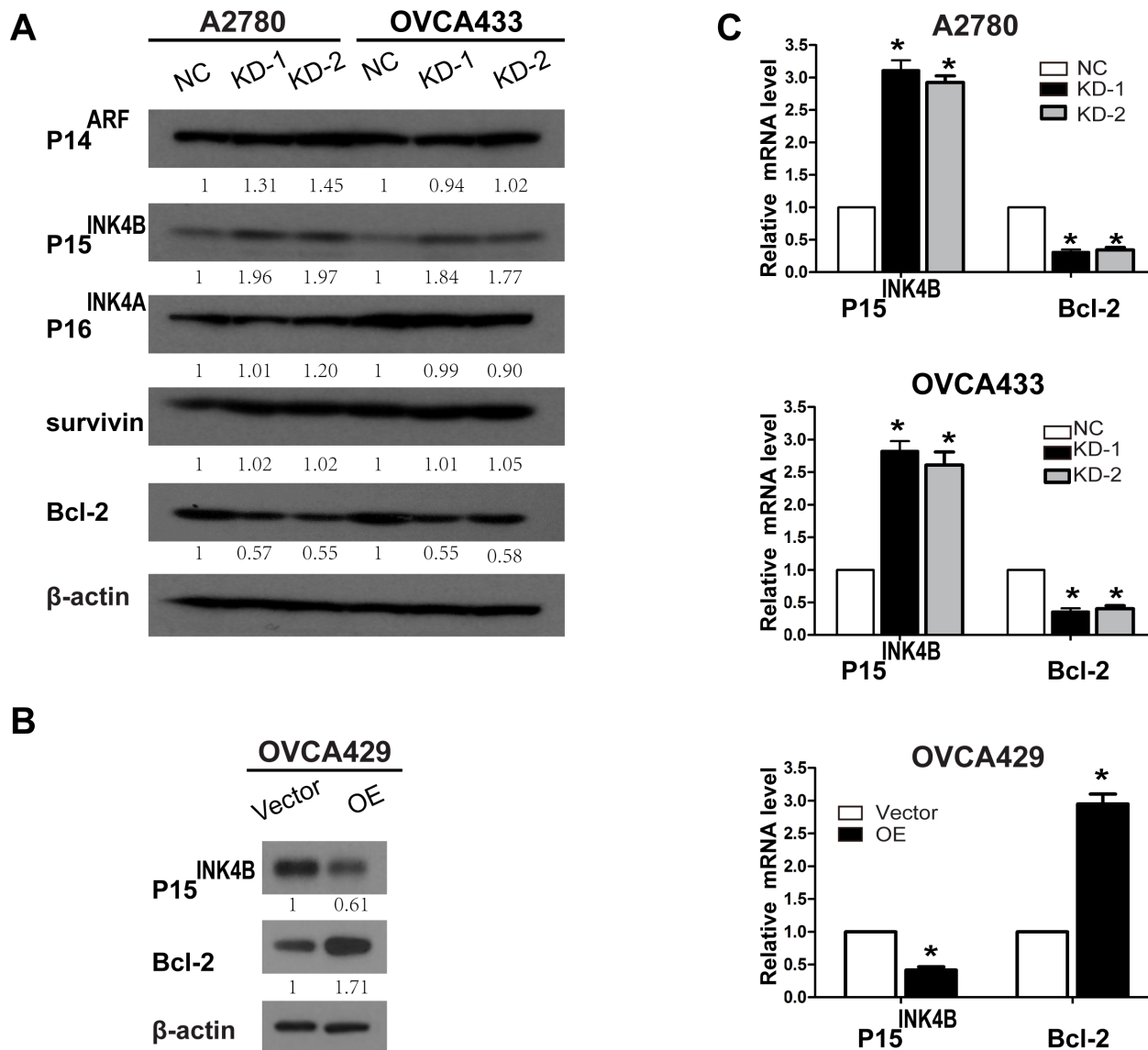


Figure 5: Knockdown and overexpression of ANRIL alters P15^{INK4B} and Bcl-2 expression. (A) Western blots showing that ANRIL knockdown increases P15^{INK4B} and decreases Bcl-2 levels in A2780 and OVCA433 cells. (B) Western blots showing that overexpression of ANRIL decreases P15^{INK4B} and increases Bcl-2 protein levels in OVCA429 cells. (C) Increased P15^{INK4B} and decreased Bcl-2 mRNA levels were detected by qRT-PCR in A2780-KD and OVCA433-KD cells while decreased P15^{INK4B} and increased Bcl-2 mRNA levels were detected in OVCA429-OE cells.

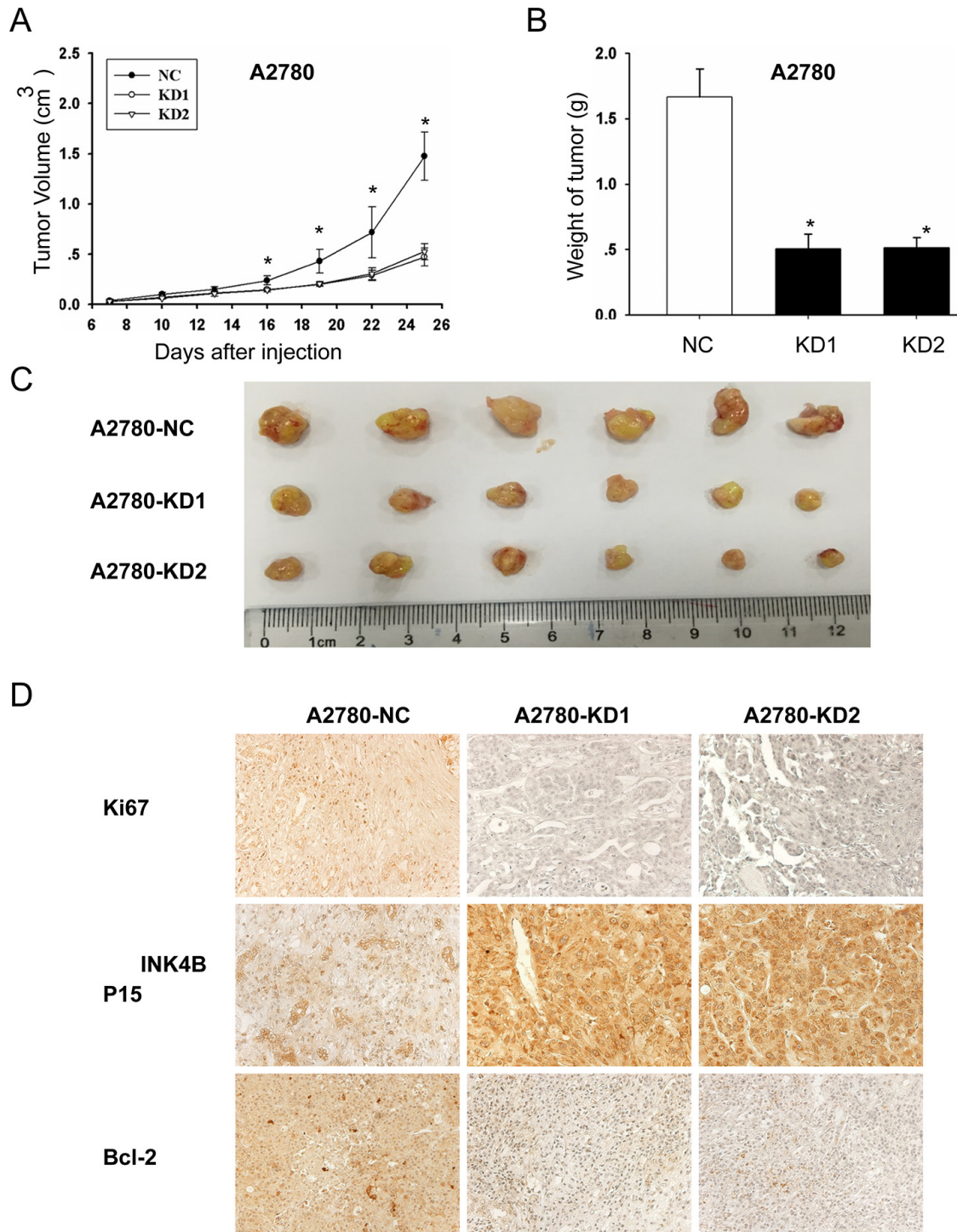


Figure 6: ANRIL knockdown inhibits A2780 cell proliferation *in vivo*. (A) Growth curves of tumor xenografts. The volumes of tumors originating from A2780-KD1 and A2780-KD2 cells were substantially smaller than those originating from A2780-NC cells, and the size difference between the two groups increased over time (six mice per group; $*P < 0.05$). (B) The weights of the A2780-NC tumors were significantly greater than those of the A2780-KD1 and A2780-KD2 tumors. $*P < 0.05$. (C) Representative images of tumors in nude mice after subcutaneous injection of A2780-NC, A2780-KD1, and A2780-KD2 cells. (D) Immunohistochemical staining showing that tumors originating from A2780-KD1 and A2780-KD2 cells had increased P15^{INK4B} and decreased ki67 and Bcl-2 levels compared to those originating from A2780-NC cells.

MATERIALS AND METHODS

Patients and tissue samples

This study was authorized by the Research Ethics Committee of Fudan University, China. All patients agreed to the procedure and signed consent forms. All specimens were handled according to ethical and legal standards.

The study consisted of 102 EOC tissues, including 68 SOC tissues that were part of our previous study [29], 20 mucinous ovarian cancer tissues, and 14 endometrioid ovarian cancer tissues that were obtained from the Tissue Bank of the Obstetrics and Gynecology Hospital of Fudan University. All specimens were surgically resected from patients who were admitted to the Department of Gynecology at the Obstetrics and Gynecology Hospital of Fudan University between August 2005 and December 2008. All EOC tissues were selected from patients who (a) did not receive preoperative radiotherapy, chemotherapy, or hormonal therapy; and (b) did not have borderline ovarian tumors or two or more different malignancies. Thirty normal ovarian epithelial tissues were obtained from participants diagnosed with uterine fibroids who were scheduled to undergo a hysterectomy and oophorectomy. Tissues were selected from participants who did not have a history of ovarian cysts, ovarian pathology, or ovarian surgery. All samples were immediately frozen in liquid nitrogen and stored at -80°C until use.

The clinicopathological characteristics of all 102 EOC patients including age, histological subtype, International Federation of Gynecologists and Obstetricians (FIGO) stage, histological grade, residual tumor diameter, serum CA-125 level, and the presence of ascites were extracted from medical charts and original pathology reports. The tumor stage and histological grade diagnoses were determined according to the criteria established by the FIGO and the World Health Organization. Follow-up data were obtained by reviewing outpatient charts or via correspondence. OS was defined as the interval between the date of surgery and the date of death or the end of follow-up (January 2013).

Cell lines and cell culture

The SKOV3, OVCAR3, A2780, Hey, OVCA429, and OVCA433 human EOC cell lines were gifts from the University of Texas M.D. Anderson Cancer Center (Houston, TX, USA). A2780, Hey, SKOV3, OVCA429, and OVCA433 cells were cultured in RPMI-1640 (Gibco, Gaithersburg, MD, USA). OVCAR3 cells were maintained in McCoy's 5A (modified) medium in humidified air at 37°C in a 5% CO_2 atmosphere. All media were supplemented with 10% fetal bovine serum (FBS; Gibco), 2 mM L-glutamine, 100 U/mL penicillin, and 100 mg/mL streptomycin.

Quantitative real-time polymerase chain reaction (qRT-PCR)

Total RNA was isolated from tissues or cells using TRIzol reagent (Invitrogen, Carlsbad, CA, USA) and reverse transcribed into cDNA using an ExScript RT-PCR kit (TaKaRa, Otsu, Japan) according to the manufacturer's instructions. The qRT-PCR reactions were performed using an ABI7500 System (Applied Biosystems, Foster City, CA, USA) and SYBR Green PCR Master Mix (TaKaRa). ANRIL expression was measured using the following primers: forward, 5'-TGTA CTTAACCCTGGACTACCTGCC-3' and reverse, 5'-C ATTCTGATTCAACAGCAGAGATCAAAG-3'. GAPDH expression was used as an internal control and was measured with the following primers: forward, 5'-GTCAACGGATTGGTCTGTATT-3' and reverse, 5'-AGTCTTCTGGGTGGCAGTGAT-3'. All assays were performed in triplicate. Statistical analyses of the results were performed using the $2^{-\Delta\Delta\text{Ct}}$ relative quantification method.

Establishment of stable cell lines in which ANRIL was overexpressed or knocked down

The two siRNA sequences were the following: 5'-GCAAGAAACATTGCTGCTAGC-3' (ANRIL-si1) and 5'-GCCCAATTATGCTGTGGTAAC-3' (ANRIL-si2). Lentiviral vectors encoding shRNA were designed based on the sequences of ANRIL-si1 and ANRIL-si2 to knock down ANRIL expression (ANRIL-knockdown, KD1 and KD2). These vectors were constructed by Hanyin Co. (Shanghai, China). The recombinant lentiviruses (KD1 and KD2) and the negative control (NC) lentivirus (Hanyin Co.) were prepared and titered to 10^9 transfection units (TU)/mL. To obtain stable cell lines, A2780 and OVCA433 cells were seeded in six-well plates and infected with virus and polybrene the following day. Positive clones were selected with puromycin (2 $\mu\text{g}/\text{mL}$ and 5 $\mu\text{g}/\text{mL}$ for A2780 and OVCA433 cells, respectively) for 14 days to establish the following new stable cell lines: A2780-NC, A2780-KD1, A2780-KD2, OVCA433-NC, OVCA433-KD1, and OVCA433-KD2 cells. Additionally, the lentiviruses expressing the ANRIL sequence (ANRIL-overexpression, OE) and the negative control lentivirus (Vector) were constructed by Hanyin Co. (Shanghai, China). ANRIL-OE and control stable cell lines (OVCA429-OE, OVCA429-vector cells) were then established. The efficiency of ANRIL knockdown and overexpression was confirmed by qRT-PCR.

Cell proliferation assays

A total of 3,000 A2780 cells, 1,000 OVCA433 cells, and 1,000 OVCA429 cells in 200 μL of medium were incubated in 96-well culture plates. Cell proliferation

was assayed using a 3-(4, 5-dimethylthiazol-2-yl)-2, 5-diphenyltetrazolium bromide (MTT) kit (Sigma-Aldrich, St. Louis, MO, USA) and a Synergy H4 Hybrid Reader. Briefly, the culture medium was removed after 1, 2, 3, 4, and 5 days, and 0.5 mg/mL MTT in 200 μ L of medium was added to each well and incubated for 4 h. The cells were then treated with 150 μ L DMSO for 10 min, and the optical density (OD) measured at 540 nm. Each experiment was repeated in triplicate.

Colony formation assays

A total of 500 A2780 cells, 150 OVCA433 cells, and 150 OVCA429 cells were plated in six-well plates. Duplicate cultures of each cell type were maintained at 37°C in a 5% CO₂ atmosphere, and fresh medium was added every 3 days. After 2 weeks, colonies consisting of > 50 cells in each well were counted. Each experiment was repeated in triplicate.

Cell cycle and apoptosis analysis

For cell cycle analysis, 2 \times 10⁶ cells were harvested, fixed with 4 mL of cold 75% ethanol at -20°C overnight, and washed twice with PBS. The cells were then resuspended in 500 μ L of PBS and simultaneously stained with 200 μ L of propidium iodide (50 μ L/mL; Sigma-Aldrich) and incubated with 20 μ L of RNase (1 mg/mL; Sigma-Aldrich) in a 37°C water bath for 15–20 min. The percentage of cells in each phase of the cell cycle was determined using a FACStation (FV500, Beckman Coulter, Brea, CA, USA) and analyzed using the Kaluza[®] Flow Analysis Software. Each experiment was repeated in triplicate.

For apoptosis analyses, 1 \times 10⁵ cells were stained with Annexin V and propidium iodide using an Annexin V-APC kit (BD Pharmingen[™] catalog number 550474, BD Biosciences, Franklin Lakes, NJ, USA) and analyzed with a FACStation equipped with CellQuest software. Each experiment was repeated in triplicate.

β -galactosidase senescence assays

A total of 1 \times 10⁶ A2780 cells, 4 \times 10⁵ OVCA433 cells, and 4 \times 10⁵ OVCA429 cells were cultured in a 6-cm dish and incubated for 3 days in RPMI-1640 medium supplemented with 10% FBS. When the cells reached approximately 80% confluence, they were fixed and incubated with a freshly prepared senescence-associated β -galactosidase staining solution in the dark at 37°C overnight. The percentage of cells that were positive for β -galactosidase activity was determined by counting the number of blue cells in 10 fields at 20 \times magnification. Each experiment was repeated in triplicate.

Western blotting

Western blotting was performed as previously described [34]. Primary antibodies against the following proteins were obtained from Santa Cruz Biotechnology (Santa Cruz, CA, USA): P14^{ARF}, P15^{INK4B}, P16^{INK4A}, Bcl-2, survivin, caspase-9, caspase-3, and caspase-7. β -actin (A2228, Sigma-Aldrich) was used as a loading control. The secondary antibodies were F(ab)₂ fragments of donkey anti-mouse immunoglobulin or donkey anti-rabbit immunoglobulin linked to horseradish peroxidase (Cell Signaling Technology, Beverly, MA, USA). Immunoblotting reagents from an electrochemiluminescence kit were used (Amersham Biosciences, Uppsala, Sweden).

Xenograft tumors in nude mice

The animal experiments were approved by the Institutional Animal Care and Use Committee of Fudan University and were performed according to the institutional guidelines and protocols. Female BALB/c athymic nude mice (4–6 weeks old weighing 20–22 g) were provided by the Department of Laboratory Animals of Fudan University and housed in a pathogen-free animal facility. To generate tumor growth *in vivo*, 1 \times 10⁶ A2780-KD1, A2780-KD2, and A2780-NC cells were subcutaneously injected into the mice (n = 6 for each cell line). The tumor volume was calculated as previously described [45]. Once a tumor reached 1.0 cm in diameter, the mice were euthanized and the tumors weighed.

Statistical analyses

All statistical analyses were performed using SPSS for Windows v.16.0 (SPSS, Chicago, IL, USA). Continuous data were analyzed using an independent *t*-test between two groups. Categorical data were analyzed using the chi-square test or Fisher's exact test as appropriate. OS rates were calculated using the Kaplan-Meier method and the log-rank test for comparisons. Multivariate survival analyses were performed on all factors that were significant in univariate analyses using the Cox regression model. *P* values < 0.05 were considered significant (P < 0.05).

FINANCIAL SUPPORT

This project was sponsored by the National Natural Science Foundation of China (81370689 and 81571404; to Ke Qin Hua), the National Natural Science Foundation of China (81502240; to Jun jun Qiu), the Shanghai Sailing Program (15YF1401400; to Jun jun Qiu), and the National Natural Science Foundation of China (81502049 to Yan Wang and 81402152 to Ying Zhang).

CONFLICTS OF INTEREST

The authors have no conflicts of interest to declare.

REFERENCES

1. Jemal A, Bray F, Center MM, Ferlay J, Ward E, Forman D. Global cancer statistics. *CA Cancer J Clin.* 2011; 61:69–90. doi: 10.3322/caac.20107.
2. Siegel R, Naishadham D, Jemal A. Cancer statistics, 2012. *CA Cancer J Clin.* 2012; 62:10–29. doi: 10.3322/caac.20138.
3. Bast RC Jr, Hennessy B, Mills GB. The biology of ovarian cancer: new opportunities for translation. *Nat Rev Cancer.* 2009; 9:415–428. doi: 10.1038/nrc2644.
4. Bowtell DD. The genesis and evolution of high-grade serous ovarian cancer. *Nat Rev Cancer.* 2010; 10:803–808. doi: 10.1038/nrc2946.
5. Rustin G, van der Burg M, Griffin C, Qian W, Swart AM. Early versus delayed treatment of relapsed ovarian cancer. *Lancet.* 2011; 377:380–381. doi: 10.1016/S0140-6736:60126-8.
6. ENCODE Project Consortium, Birney E, Stamatoyannopoulos JA, Dutta A, Guigó R, Gingeras TR, Margulies EH, Weng Z, Snyder M, Dermitzakis ET, Thurman RE, Kuehn MS, Taylor CM, et al. Identification and analysis of functional elements in 1% of the human genome by the ENCODE pilot project. *Nature.* 2007; 447:799–816. doi: 10.1038/nature05874.
7. Kapranov P, St Laurent G, Raz T, Ozsolak F, Reynolds CP, Sorensen PH, Reaman G, Milos P, Arceci RJ, Thompson JF, Triche TJ. The majority of total nuclear-encoded non-ribosomal RNA in a human cell is ‘dark matter’ un-annotated RNA. *BMC Biol.* 2010; 8:149. doi: 10.1186/1741-7007-8-149.
8. Matouk IJ, DeGroot N, Mezan S, Ayesh S, Abu-lail R, Hochberg A, Galun E. The H19 non-coding RNA is essential for human tumor growth. *PLOS ONE.* 2007; 2:e845. doi: 10.1371/journal.pone.0000845.
9. Gupta RA, Shah N, Wang KC, Kim J, Horlings HM, Wong DJ, Tsai MC, Hung T, Argani P, Rinn JL, Wang Y, Brzoska P, Kong B, et al. Long non-coding RNA HOTAIR reprograms chromatin state to promote cancer metastasis. *Nature.* 2010; 464:1071–1076. doi: 10.1038/nature08975.
10. Gutschner T, Hämmerle M, Eissmann M, Hsu J, Kim Y, Hung G, Revenko A, Arun G, Stentrup M, Gross M, Zörnig M, MacLeod AR, Spector DL, et al. The noncoding RNA MALAT1 is a critical regulator of the metastasis phenotype of lung cancer cells. *Cancer Res.* 2013; 73:1180–1189. doi: 10.1158/0008-5472.CAN-12-2850.
11. Du Y, Kong G, You X, Zhang S, Zhang T, Gao Y, Ye L, Zhang X. Elevation of highly up-regulated in liver cancer (HULC) by hepatitis B virus x protein promotes hepatoma cell proliferation via down-regulating p18. *J Biol Chem.* 2012; 287:26302–26311. doi: 10.1074/jbc.M112.342113.
12. Zhou Y, Zhang X, Klibanski A. MEG3 noncoding RNA: a tumor suppressor. *J Mol Endocrinol.* 2012; 48:R45–R53. doi: 10.1530/JME-12-0008.
13. Lu X, Fang Y, Wang Z, Xie J, Zhan Q, Deng X, Chen H, Jin J, Peng C, Li H, Shen B. Downregulation of gas5 increases pancreatic cancer cell proliferation by regulating CDK6. *Cell Tissue Res.* 2013; 354:891–896. doi: 10.1007/s00441-013-1711-x.
14. Yuan SX, Yang F, Yang Y, Tao QF, Zhang J, Huang G, Yang Y, Wang RY, Yang S, Huo XS, Zhang L, Wang F, Sun SH, et al. Long noncoding RNA associated with microvascular invasion in hepatocellular carcinoma promotes angiogenesis and serves as a predictor for hepatocellular carcinoma patients’ poor recurrence-free survival after hepatectomy. *Hepatology.* 2012; 56:2231–2241. doi: 10.1002/hep.25895.
15. Huarte M, Guttman M, Feldser D, Garber M, Koziol MJ, Kenzelmann-Broz D, Khalil AM, Zuk O, Amit I, Rabani M, Attardi LD, Regev A, Lander ES, et al. A large intergenic noncoding RNA induced by p53 mediates global gene repression in the p53 response. *Cell.* 2010; 142:409–419. doi: 10.1016/j.cell.2010.06.040.
16. Quagliata L, Matter MS, Piscuoglio S, Arabi L, Ruiz C, Procino A, Kovac M, Moretti F, Makowska Z, Boldanova T, Andersen JB, Hämmerle M, Tornillo L, et al. Long noncoding RNA HOTTIP/HOXA13 expression is associated with disease progression and predicts outcome in hepatocellular carcinoma patients. *Hepatology.* 2014; 59:911–923. doi: 10.1002/hep.26740.
17. Ge X, Chen Y, Liao X, Liu D, Li F, Ruan H, Jia W. Overexpression of long noncoding RNA PCAT-1 is a novel biomarker of poor prognosis in patients with colorectal cancer. *Med Oncol.* 2013; 30:588. doi: 10.1007/s12032-013-0588-6.
18. Tano K, Akimitsu N. Long non-coding RNAs in cancer progression. *Front Genet.* 2012; 3:219. doi: 10.3389/fgene.2012.00219.
19. Pasmant E, Laurendeau I, Héron D, Vidaud M, Vidaud D, Bièche I. Characterization of a germ-line deletion, including the entire INK4/ARF locus, in a melanoma-neural system tumor family: identification of ANRIL, an antisense noncoding RNA whose expression coclusters with ARF. *Cancer Res.* 2007; 67:3963–3969. doi: 10.1158/0008-5472.CAN-06-2004.
20. Turnbull C, Ahmed S, Morrison J, Pernet D, Renwick A, Maranian M, Seal S, Ghoussaini M, Hines S, Healey CS, Hughes D, Warren-Perry M, Tapper W, et al. Genome-wide association study identifies five new breast cancer susceptibility loci. *Nat Genet.* 2010; 42:504–507. doi: 10.1038/ng.586.
21. Chen J, Li D, Wei C, Sen S, Killary AM, Amos CI, Evans DB, Abbruzzese JL, Frazier ML. Aurora-A and p16 polymorphisms contribute to an earlier age at diagnosis of pancreatic cancer in Caucasians. *Clin Cancer Res.* 2007; 13:3100–3104. doi: 10.1158/1078-0432.CCR-06-2319.

22. Bei JX, Li Y, Jia WH, Feng BJ, Zhou G, Chen LZ, Feng QS, Low HQ, Zhang H, He F, Tai ES, Kang T, Liu ET, et al. A genome-wide association study of nasopharyngeal carcinoma identifies three new susceptibility loci. *Nat Genet.* 2010; 42:599–603. doi: 10.1038/ng.601.
23. Stacey SN, Sulem P, Masson G, Gudjonsson SA, Thorleifsson G, Jakobsdottir M, Sigurdsson A, Gudbjartsson DF, Sigurgeirsson B, Benediktsdottir KR, Thorisdottir K, Ragnarsson R, Scherer D, et al. New common variants affecting susceptibility to basal cell carcinoma. *Nat Genet.* 2009; 41:909–914. doi: 10.1038/ng.412.
24. Rajaraman P, Melin BS, Wang Z, McKean-Cowdin R, Michaud DS, Wang SS, Bondy M, Houlston R, Jenkins RB, Wrensch M, Yeager M, Ahlbom A, Albanes D, et al. Genome-wide association study of glioma and meta-analysis. *Hum Genet.* 2012; 131:1877–1888. doi: 10.1007/s00439-012-1212-0.
25. Sherborne AL, Hosking FJ, Prasad RB, Kumar R, Koehler R, Vijayakrishnan J, Papaemmanuil E, Bartram CR, Stanulla M, Schrappe M, Gast A, Dobbins SE, Ma Y, et al. Variation in CDKN2A at 9p21.3 influences childhood acute lymphoblastic leukemia risk. *Nat Genet.* 2010; 42:492–494. doi: 10.1038/ng.585.
26. Yap KL, Li S, Muñoz-Cabello AM, Raguz S, Zeng L, Mujtaba S, Gil J, Walsh MJ, Zhou MM. Molecular interplay of the noncoding RNA ANRIL and methylated histone H3 lysine 27 by polycomb CBX7 in transcriptional silencing of INK4a. *Mol Cell.* 2010; 38:662–674. doi: 10.1016/j.molcel.2010.03.021.
27. Chen D, Zhang Z, Mao C, Zhou Y, Yu L, Yin Y, Wu S, Mou X, Zhu Y. ANRIL inhibits p15 (INK4b) through the TGFβ1 signaling pathway in human esophageal squamous cell carcinoma. *Cell Immunol.* 2014; 289:91–96. doi: 10.1016/j.cellimm.2014.03.015.
28. Zhang EB, Kong R, Yin DD, You LH, Sun M, Han L, Xu TP, Xia R, Yang JS, De W, Chen Jf. Long noncoding RNA ANRIL indicates a poor prognosis of gastric cancer and promotes tumor growth by epigenetically silencing of miR-99a/miR-449a. *Oncotarget.* 2014; 5:2276–2292. doi: 10.18632/oncotarget.1902.
29. Qiu JJ, Lin YY, Ding JX, Feng WW, Jin HY, Hua KQ. Long non-coding RNA ANRIL predicts poor prognosis and promotes invasion/metastasis in serous ovarian cancer. *Int J Oncol.* 2015; 46:2497–2505. doi: 10.3892/ijo.2015.2943.
30. Gil J, Peters G. Regulation of the INK4b-ARF-INK4a tumour suppressor locus: all for one or one for all. *Nat Rev Mol Cell Biol.* 2006; 7:667–677. doi: 10.1038/nrm1987.
31. Wang Y, Wang Z, Qi Z, Yin S, Zhang N, Liu Y, Liu M, Meng J, Zang R, Zhang Z, Yang G. The negative interplay between Aurora A/B and BRCA1/2 controls cancer cell growth and tumorigenesis via distinct regulation of cell cycle progression, cytokinesis, and tetraploidy. *Mol Cancer.* 2014; 13:94. doi: 10.1186/1476-4598-13-94.
32. Liu Z, Zhang X, Xu X, Chen L, Li W, Yu H, Sun Y, Zeng J, Jia J. RUNX3 inhibits survivin expression and induces cell apoptosis in gastric cancer. *Eur J Cell Biol.* 2014; 93:118–126. doi: 10.1016/j.ejcb.2014.02.002.
33. Zhu H, Li X, Song Y, Zhang P, Xiao Y, Xing Y. Long non-coding RNA ANRIL is up-regulated in bladder cancer and regulates bladder cancer cell proliferation and apoptosis through the intrinsic pathway. *Biochem Biophys Res Commun.* 2015; 467:223–228.
34. Qiu JJ, Lin YY, Ye LC, Ding JX, Feng WW, Jin HY, Zhang Y, Li Q, Hua KQ. Overexpression of long non-coding RNA HOTAIR predicts poor patient prognosis and promotes tumor metastasis in epithelial ovarian cancer. *Gynecol Oncol.* 2014; 134:121–128. doi: 10.1016/j.ygyno.2014.03.556.
35. Yang Z, Zhou L, Wu LM, Lai MC, Xie HY, Zhang F, Zheng SS. Overexpression of long non-coding RNA HOTAIR predicts tumor recurrence in hepatocellular carcinoma patients following liver transplantation. *Ann Surg Oncol.* 2011; 18:1243–1250. doi: 10.1245/s10434-011-1581-y.
36. Kogo R, Shimamura T, Mimori K, Kawahara K, Imoto S, Sudo T, Tanaka F, Shibata K, Suzuki A, Komune S, Miyano S, Mori M. Long noncoding RNA HOTAIR regulates polycomb-dependent chromatin modification and is associated with poor prognosis in colorectal cancers. *Cancer Res.* 2011; 71:6320–6326. doi: 10.1158/0008-5472.CAN-11-1021.
37. Niinuma T, Suzuki H, Nojima M, Noshio K, Yamamoto H, Takamaru H, Yamamoto E, Maruyama R, Nobuoka T, Miyazaki Y, Nishida T, Bamba T, Kanda T, et al. Upregulation of miR-196a and HOTAIR drive malignant character in gastrointestinal stromal tumors. *Cancer Res.* 2012; 72:1126–1136. doi: 10.1158/0008-5472.CAN-11-1803.
38. Kim K, Jutooru I, Chadalapaka G, Johnson G, Frank J, Burghardt R, Kim S, Safe S. HOTAIR is a negative prognostic factor and exhibits pro-oncogenic activity in pancreatic cancer. *Oncogene.* 2013; 32:1616–1625. doi: 10.1038/onc.2012.193.
39. Tu ZQ, Li RJ, Mei JZ, Li XH. Down-regulation of long non-coding RNA GAS5 is associated with the prognosis of hepatocellular carcinoma. *Int J Clin Exp Pathol.* 2014; 7:4303–4309.
40. Yin D, He X, Zhang E, Kong R, De W, Zhang Z. Long noncoding RNA GAS5 affects cell proliferation and predicts a poor prognosis in patients with colorectal cancer. *Med Oncol.* 2014; 31:253. doi: 10.1007/s12032-014-0253-8.
41. Sato K, Nakagawa H, Tajima A, Yoshida K, Inoue I. ANRIL is implicated in the regulation of nucleus and potential transcriptional target of E2F1. *Oncol Rep.* 2010; 24:701–707.
42. Congrains A, Kamide K, Katsuya T, Yasuda O, Oguro R, Yamamoto K, Ohishi M, Rakugi H. CVD-associated non-coding RNA, ANRIL, modulates expression of atherogenic pathways in VSMC. *Biochem Biophys*

- Res Commun. 2012; 419:612–616. doi: 10.1016/j.bbrc.2012.02.050.
43. Kotake Y, Nakagawa T, Kitagawa K, Suzuki S, Liu N, Kitagawa M, Xiong Y. Long non-coding RNA ANRIL is required for the PRC2 recruitment to and silencing of p15 (INK4B) tumor suppressor gene. *Oncogene*. 2011; 30:1956–1962. doi: 10.1038/onc.2010.568.
44. Xia DY, Liu L, Hao MW, Liu Q, Chen RA, Liang YM. A combination of STI571 and BCR-ABL1 siRNA with overexpressed p15INK4B induced enhanced proliferation inhibition and apoptosis in chronic myeloid leukemia. *Braz J Med Biol Res*. 2014; 47:1096–1101.
45. Wang Y, Wang Z, Qi Z, Yin S, Zhang N, Liu Y, Liu M, Meng J, Zang R, Zhang Z, Yang G. The negative interplay between Aurora A/B and BRCA1/2 controls cancer cell growth and tumorigenesis via distinct regulation of cell cycle progression, cytokinesis, and tetraploidy. *Mol Cancer*. 2014; 13:94. doi: 10.1186/1476-4598-13-94.